Direct measurement of small particle growth and aging at SGP

Final report

Principal Investigator:

Don Collins
donc@ucr.edu

DOE Grant: DE-SC0018970

DOE/Office of Science Program Office: Office of Biological and Environmental Research

Abstract

Atmospheric aerosols influence climate directly by scattering and absorbing solar radiation and indirectly through their influence on the reflectivity and lifetime of clouds. But that influence is limited to only those particles large enough to efficiently interact with solar radiation (diameter, $D_p \gtrsim 100$ nm) and/or to form cloud droplets at typical atmospheric supersaturations ($D_p \gtrsim 50$ nm). Many cloud condensation nuclei (CCN) originate as ~1 nm nucleated particles that must grow to those threshold sizes before being lost to coagulation with larger particles. Though there is consensus that new particle formation and growth contributes significantly to total CCN concentrations, different groups using different models and assumptions have arrived at diverse estimates.

To directly evaluate the rate at which small particles grow in a well-characterized environment, our research group operated two identical Captive Aerosol Growth and Evolution (CAGE) chambers at the DOE Southern Great Plains (SGP) site in the late summer and fall of 2021. CAGE chambers are designed to expose particles to an environment that mirrors that of the surroundings with or without a controlled perturbation designed to assess a sensitivity. The analysis here focuses on roughly the last two months of the overall study period during which measurements were almost continuous and when several perturbation experiments were conducted.

Though the utility of a dual-chamber system is the ability to measure the influence of a single change on top of ambient conditions, both chambers were initially operated in the same way, with ambient air pulled through the gas exchange channel in both and ammonium sulfate particles injected into both. The similar time-dependent particle growth observed in the chambers for those periods provides confidence in differences observed during the subsequent perturbation experiments. The growth rate of particles in the reference chamber into which only ammonium sulfate particles were injected and for which only ambient air was pulled through were used to describe time-of-day averages. The average growth rate was highest in the evening and in the morning after sunrise and lowest in the late afternoon.

The sensitivity of particle growth to secondary aerosol precursor gases was studied by adding them at a controlled rate to the ambient air flow pulled through one of the two chambers. Addition of 5 ppb of α-pinene resulted in an average particle growth rate of 4.4 nm/hr, compared with that of just 0.8 nm/hr in the reference chamber. The added α-pinene also triggered one new particle formation (NPF) event in the early evening just before sunset and another in the morning just after sunrise. Similarly, addition of 5 ppb of SO_2 to one chamber led to a pair of NPF events and to increased particle growth rate, though unlike the impact of added α-pinene, growth was enhanced only during the daytime when OH concentration is highest.

The influence of aerosol liquid water on secondary aerosol formation and particle growth was investigated by injecting ammonium sulfate seed particles into one chamber and potassium sulfate particles into the other. Particles were injected into the two chambers 4 times over a 1.5-day period. The chamber RH history during and following each injection was used to determine whether each particle type was crystalline or aqueous. For the case when both particle types remained crystalline throughout the period they were tracked and for that when they remained aqueous, the magnitude and time-dependence of the growth of both were almost exactly the same. For the other two cases the ammonium sulfate particles deliquesced upon injection and remained aqueous, while the potassium sulfate particles remained crystalline. For those two cases, the aqueous particles grew by an average of 0.41 and 0.41 nm/hr, while the crystalline particles grew by only 0.06 and 0.16 nm/hr.

This project supported two Ph.D. students (Xuanlin Du and Zihan Zhu), one M.S. student (Candice Sirmollo), and five undergraduates (Kyle Davis, Adriana Gueta, Diana Ibarra-Gomez, Joshua Milne, and Barbara Trujillo). The results from this work made up a major component of Dr. Zihan Zhu's dissertation, which she defended in spring 2023.

1 Background and motivation

Atmospheric aerosols influence air quality (Viana et al., 2014), human health (Pöschl, 2005), ecosystems (Cirino et al., 2014; Misson et al., 2005), and climate (Jaenicke, 1980; McNeill, 2017). Aerosols affect climate directly by absorbing and scattering solar radiation and indirectly by influencing cloud properties. Both of those effects are strongly dependent on particle size, with particles smaller than about 0.05 to 0.1 μm having limited impact because of their weak interaction with visible light and their inability to act as cloud condensation nuclei (CCN) (Seinfeld and Pandis, 2016). The concentration of CCN is significantly influenced by new particle formation (NPF) (Duplissy et al., 2016; Gordon et al., 2017; Kalivitis et al., 2015), with the contribution to the CCN budget dependent on the balance between the timescale for growth to that threshold size range and that for loss to surfaces and, especially, other particles through coagulation. Long-term observations and model simulations can provide insights into these processes. Particle formation, growth, and aging mechanisms are influenced by the types and concentrations of precursor gases and by ambient conditions, including solar intensity, temperature, and relative humidity (RH) (Kerminen, 2018). Significant variations in NPF frequency exist between different locations. For example, the NPF event frequency is reported to be as high as 86% in parts of South Africa (Hirsikko et al., 2012), while no NPF events were observed during a 3-month study in the Amazonian Forest (Wimmer et al., 2017).

Conventional approaches for studying the growth of small particles typically focus on one or a few precursor gases or rely on observations of the dynamics of ambient particle populations. Interpreting ambient aerosol observations is challenging because the measurements are affected by both gas and particle phase chemistry and by the variability in the origin and history of the air arriving at the measurement site at a given time. Descriptions of particle growth rate can also be biased growth is most easily estimated during NPF events for which limited data are available and during which atmospheric conditions are conducive for nucleation and growth (Kulmala et al., 2014). Characterizing the spatial and temporal distribution and the controls of particle formation and growth also necessitates long-term continuous measurements that encompass a wide range of conditions.

While traditional environmental chambers can provide detailed information on the species and processes involved in secondary aerosol formation and resulting particle growth, they are often restricted to narrow ranges of simulated conditions and do not capture the complexity and variability of the ambient atmosphere. The Captive Aerosol Growth and Evolution (CAGE) chamber system was developed as a complement to those traditional chambers for studying particle dynamics under atmospheric conditions at a location of interest. The system is portable and designed for field use (Sirmollo et al., 2021). Solar spectral intensity inside each of the two identical chambers mirrors that just outside, while the gas composition is either similar to that outside or is perturbed in some way through addition of one or more gases. For typical experiments, one of the two chambers serves as a reference or control and the other as a perturbation chamber to assess the sensitivity of particle growth to different parameters.

This manuscript presents the results from the first deployment of a new generation of CAGE chamber at the DOE Atmospheric Radiation Measurement (ARM) Program's Southern Great Plains (SGP) site in the late summer and fall of 2021. We describe the time-of-day dependence of the growth rate during the study

and the observed sensitivity of particle growth to the liquid water content of injected seed particles and to addition of α-pinene and sulfur dioxide (SO_2).

2 Methods

2.1 CAGE chambers

The experimental system used in this study combined two CAGE chambers (referred to as simply chamber A and chamber B) with particle generation and sampling instrumentation housed in an adjacent trailer. Figure 1 illustrates the type of CAGE chamber used at SGP. Detailed information about the characteristics and features of an earlier design of the chamber has been previously reported (Sirmollo et al., 2021). The core of each chamber is a 1.37 m diameter x 1.37 m length cylindrical reactor made of 0.05 mm UV-transmitting perfluoroalkoxy film (PFA; Saint-Gobain) with an internal volume of 2.0 m^3. The axle of the chamber is an 18 cm diameter roughly cylindrical channel that is wrapped with gas-permeable 0.005 mm expanded polytetrafluoroethylene membrane (ePTFE; Phillips Scientific). Gases diffuse through the membrane between the sealed reactor volume and the continuously ventilated interior of the channel, which is hereafter referred to as the *gas exchange channel*.

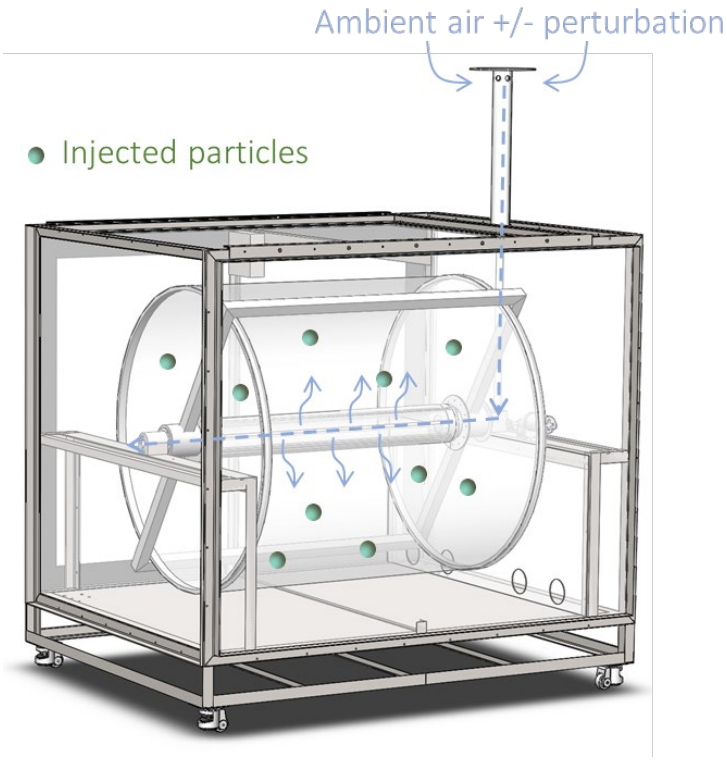

Figure 1. Sketch of a CAGE chamber showing the path of ambient air that is pulled in through an inlet, filtered, and then flows through the center of the gas exchange channel.

Each chamber is designed to pull approximately 75 L min^{-1} ambient air into a rigid PFA inlet, through an all-Teflon (PFA+PTFE) cartridge filter (Pure Process Filtration, GPFA), and then through the gas exchange channel, before being exhausted through a port connected to a variable speed blower (Ametek DFS, R304C) below the chamber. Efficient gas exchange across the ePTFE membrane allows the

chamber to maintain gas composition and concentrations close to those in the surrounding ambient air. Controlled additions of precursor or other gases can be mixed into the ambient air flow in one or both chambers. The chamber is maintained at a positive pressure differential of around 1 mbar relative to the surrounding enclosure to prevent deformation and to minimize contamination of outside particles.

As described in Sirmollo et al. (2021), trace gas concentrations in each chamber can be explained by treating the volume as a continuous stirred-tank reactor (CSTR). The resulting rate of change of the concentration of any of the trace gases can then be expressed as

$$\frac{dC_{ch}}{dt} = P - L + \frac{Q_{ex}}{V_{ch}} C_{amb} - \frac{Q_{ex}}{V_{ch}} C_{ch} \quad (1)$$

Where C_{ch} is the concentration in the chamber, C_{amb} is the ambient concentration, V_{ch} is the volume of the chamber, P and L are the per unit volume rates of chemical production and loss in the chamber, respectively, and Q_{ex} is the effective exchange "flow rate" across the ePTFE membrane. The Q_{ex} cannot be measured directly and was instead estimated using Eq. (1) and the time series of SO_2 concentration measured in one of the chambers during an experiment in which step changes in concentration were introduced into the ambient air flow. The resulting Q_{ex} of about 24 L min^{-1} results in a V_{ch}/Q_{ex} = 85 min turnover time.

Size selected particles are injected into each chamber using an aerosol generation system that will be introduced in the next section. The injected particles grow and their composition changes in response to their exposure to air and environmental conditions that track those of the surroundings. NPF events sometimes occur in the chambers and add to the population of captive particles. Small volumes of chamber air are intermittently sampled to measure the size distribution, properties, and/or composition of the captive particles. Details of the particle measurements made during the study described here are provided in the next section. To minimize losses of large particles due to gravitational settling and small particles due to convective eddies, the chambers are rotated similar to rotating drums (e.g., Goldberg et al., 1971) at approximately 3 rpm using a fixed speed motor (Dayton, 1LPZ1) and a pair of sprockets.

The PFA chambers are suspended within rectangular enclosures that act to protect the PFA film and keep it clean. Each enclosure frame is constructed of stainless steel and powder coated with glossy white paint (Tiger Drylac). UV-transmitting acrylic sheets (Spartech-Polycast) are sealed against the stainless steel frames using PTFE gasket tape (Inertech, UHF). A variable speed blower (Ametek DFS, R304C) pulls air from inside the enclosure to create a slight vacuum around the chamber so that it remains taut even though the pressure inside it is slightly below ambient due to pressure drop through the inlet filter and tube. The surface below the cylindrical chamber is covered by a UV- and visible light-reflective PTFE gasket sheet (Inertech, SQ-S) to reflect some incident solar radiation back into the chamber from below to partially compensate for attenuation through the acrylic and PFA. The close relationship between the spectral intensity in the chambers and that just outside is evident in Figure 2, which shows a comparison of the cosine-weighted solar spectral intensity measured outside and at a point between the bottom of one of the chambers and the reflective PTFE gasket.

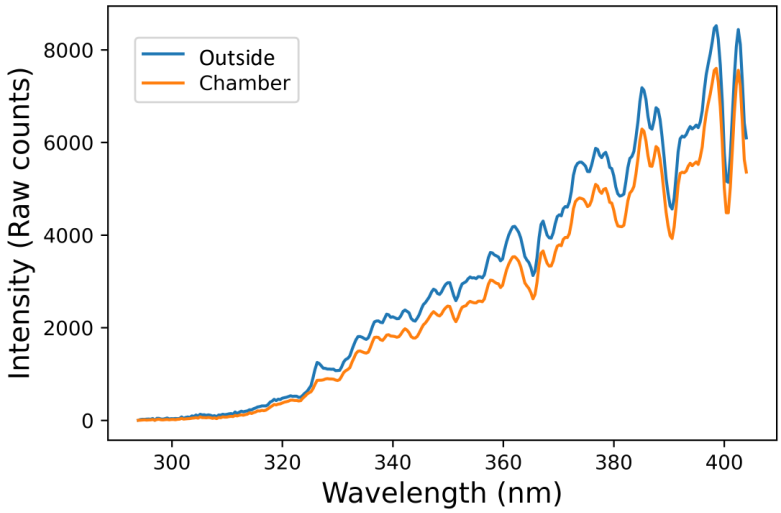

Figure 2. Comparison of spectral intensity measured just below one of the chambers and just outside of the chamber enclosure at noon on November 6, 2021.

Two thermistors inside each chamber enclosure and two just outside were used to monitor temperatures. During the project at SGP, small air conditioners with variable speed compressors (Rigid HVAC, DV3220E) were used in an attempt to cool the enclosures during the daytime to match the temperature of the surroundings. The cooling capacity of the air conditioners was found to be insufficient and they have since been replaced with external chillers that circulate cold water through heat exchangers in the chamber enclosures. During the SGP project, the average temperature inside each chamber was maintained within 5 °C of the outside temperature.

2.2 Measurement site

The CAGE chambers were operated at SGP from August 9 to November 20, 2021, though the analysis here is focused mostly on the second half of that period. The site is located in northern Oklahoma (36.607322, -97.487643) near cattle pastures and wheat fields. Regional and local satellite images and a photo of the chambers positioned outside of the instrumentation trailer are shown in Figure 3.

Figure 3. (a) Regional satellite image of the Southern Great Plains (SGP) site in northern Oklahoma, (b) satellite image of a portion of the SGP site that includes the location of the chambers. Map data © 2022

Google. (c) Photo of the two chambers positioned outside of the trailer that housed the supporting instrumentation.

2.3 Supporting instrumentation

The configuration for the dual-chamber experimental system is shown in Figure 4. The CAGE chambers were positioned outside of the former Aerosol Observing System (AOS) trailer and the sampling, aerosol generation, and trace gas perturbation equipment was located inside. The particle injection and sampling tubes were stainless steel (~5 m long x 0.95 cm outer diameter), while the gas injection and sampling lines were PFA (also ~5 m long x 0.95 cm outer diameter).

Monodisperse seed particles were produced by atomizing an ammonium sulfate or, for select periods, potassium sulfate solution using an atomizer (TSI, 3076), drying using a silica gel diffusion dryer, and separating a narrow size range at approximately 0.07 μm dry diameter, D_p, with a differential mobility analyzer (DMA) operated as an electrostatic classifier. A new particle mode was injected into each chamber as soon as the previous one became difficult to track due to decreased concentration caused by losses to the walls and to sample extraction. As described by Sirmollo et al. (2021), an additional particle mode centered at 0.3 μm D_p was repeatedly injected at a rate sufficient to maintain a prescribed surface area concentration (20 $\mu m^2\ cm^{-3}$ early in the project and 10 $\mu m^2\ cm^{-3}$ later).

A scanning mobility particle sizer (SMPS) was used to measure particle size distributions. The system was configured to cycle between measuring from each of the two chambers and then from an ambient air inlet. The sample aerosol was dried with a Nafion tube bundle (Perma Pure, PD-070-18T) and charge neutralized with a soft x-ray neutralizer (homemade, using a Hamamatsu L12535 source). The SMPS used a high flow DMA similar to that described by Stolzenburg et al. (1998) and a TSI 3762 condensation particle counter (CPC). The dry diameter size distribution between 0.013 and 0.40 μm was measured with a scan time of 90 s.

For much of the time, one of the chambers was used as a reference or control, with only dried ammonium sulfate seed particles injected and only ambient air pulled into the inlet and through the gas exchange channel. The sensitivity of particle growth to changes in the composition of the gas or seed particles was evaluated through perturbation of the other chamber. For the study described here, seed particle perturbation experiments involved injection of ammonium sulfate particles into the reference chamber and potassium sulfate particles into the other. Gas composition perturbations included addition of a controlled amount of either α-pinene (AP) or SO_2 to the flow of ambient air pulled through one of the chambers.

Several ARM datasets were used to aid in understanding the observed growth of particles in the chambers. Ozone (O_3) and SO_2 are measured at SGP using Thermo Fisher Scientific 49C and 43i analyzers, respectively. An Aerodyne Aerosol Chemical Speciation Monitor (ACSM) provides continuous measurements of the concentrations of non-refractory submicron particulate matter including organic aerosol (OA), sulfate, nitrate, ammonium, and chloride. Meteorological parameters including surface wind speed, wind direction, air temperature, and relative humidity (RH) are recorded in the ARM Surface Meteorology Systems (MET) dataset.

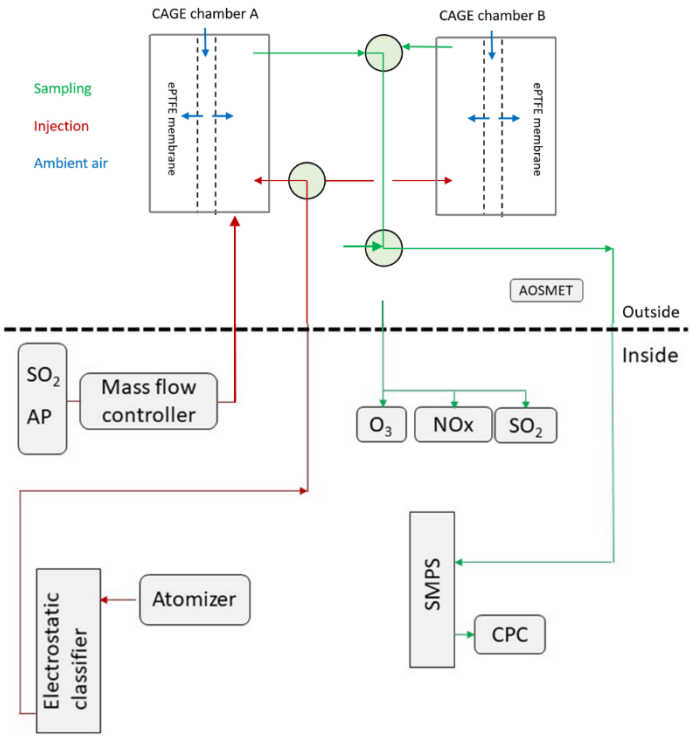

Figure 4. Schematic of the dual-chamber experimental system.

3 Results

3.1 Hourly variations of particle growth rate

Throughout the study, particle size distributions outside and inside both chambers were measured at least once per hour. The size distribution mode that began with each particle injection was tracked and fitted with a lognormal to describe the time dependence of a representative number concentration and dry diameter of the particle mode. Example results of such an analysis are provided in Figures 5 and 6. Time series of the size distributions measured in ambient air and in both chambers over a 2.5-day period in October are presented in Figure 5. During this time neither chamber was perturbed, with ambient air pulled through the gas exchange channel in both and ammonium sulfate particles injected into both. The repeating patterns evident in the chamber A and chamber B time series reflect the injections of new seed particles after the previous modes became difficult to track. The study-average particle lifetime inside the chambers was about 6 hours, with longer times at night and shorter times during the day when solar heating results in temperature gradients that promote convective mixing. The x-y representation to the left of the chamber A time series is of the size distribution measured at the time indicated by the black rectangle. The multiple peaks evident in that x-y graph and in the chamber size distribution time series graphs result from the unavoidable injection of larger particles with more than one elementary charge that are separated by the DMA together with the 0.07 μm singly charged particles.

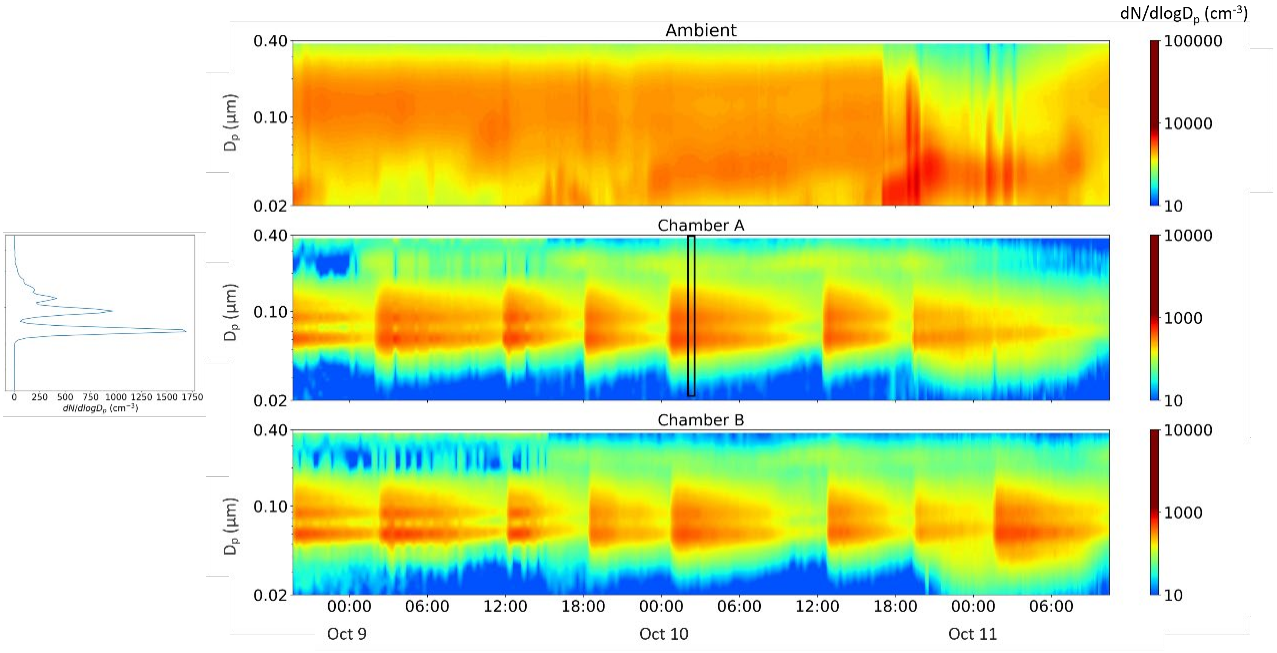

Figure 5. Top: Ambient aerosol size distribution time series from October 8 to 11. Middle and bottom: Size distribution time series over the same period in chambers A and B. Neither chamber was perturbed during this period. Left: x-y presentation of the size distribution measured at the time indicated by the black rectangle in the time series.

Time series of the mode diameters determined from the lognormal fits are shown in Figure 6, with the shaded bands indicating night time. The time-dependent growth rate for each tracked mode is calculated as the change in lognormal fit D_p between two successive measurements divided by the time difference, $\Delta D_p/\Delta t$. As expected for this case in which conditions in both chambers were the same, the time-dependent growth rates of particles in the two chambers are similar.

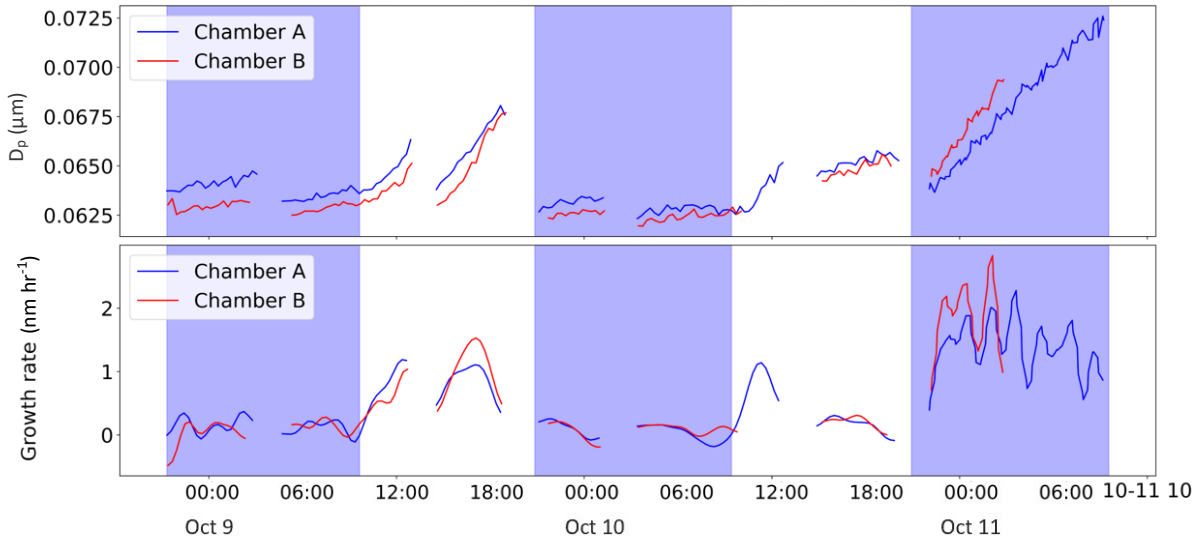

Figure 6. Top: Time series of the lognormal fit diameters of the particle modes shown in Figure 5. Bottom: Calculated growth rates for the same period.

Using measurements from the reference chamber made throughout the study, the time-of-day-dependent growth rate was calculated and is shown in Figure 7. The average growth rate remains positive throughout the day, with a minimum in the late afternoon before sunset and maxima in the evening and in the morning after sunrise. The general pattern is somewhat similar to that observed using a previous version of the CAGE chamber at a forested site north of Houston, TX in the late summer and early fall of 2016 (Sirmollo et al., 2021), though the growth rates at SGP in the fall were significantly lower. Particle growth at night was comparable to that during the day. Though regional NPF typically happens in the daytime because of photochemistry, several studies have reported various pathways contributing to nighttime particle growth, including formation of highly functionalized organonitrates (ON) from reaction of volatile organic compounds (VOC) with nitrate radical (Huang et al., 2019) and formation of semi-volatile oxygenated organic aerosol (SV-OOA) and highly oxygenated organic molecules (HOMs) (Hao et al., 2018). A significant HOM fraction was reported to be contained in submicron OA measured at SGP (Liu et al., 2021). Ammonium nitrate (NH_4NO_3) is an important component of the aerosol at SGP in part because of abundant ammonia (NH_3) from agricultural emissions (Parworth et al., 2015) and enhanced partitioning of it into the aerosol phase as temperature decreases at night may also explain some of the observed growth.

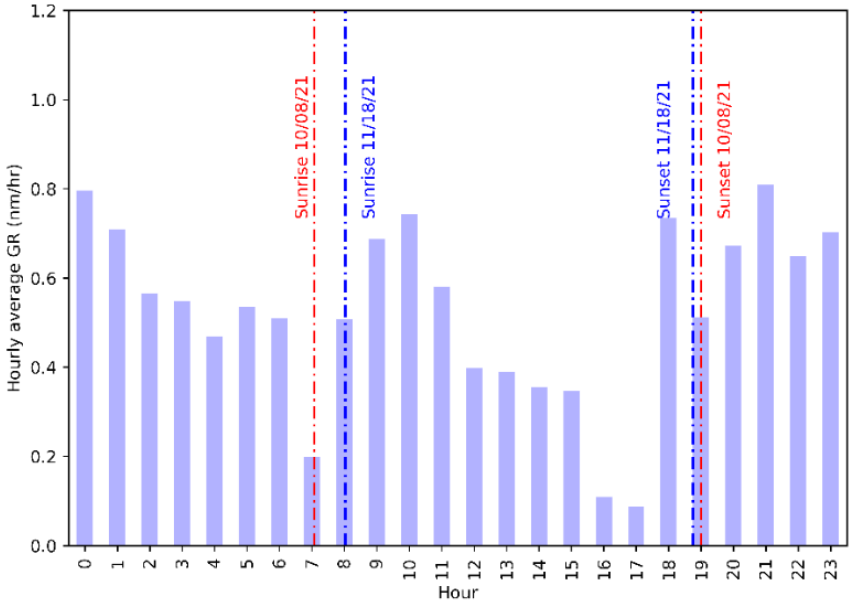

Figure 7. Time-of-day average particle growth rate. A total of 1212 values were used to calculate the averages. The time of sunrise and sunset for the first (October 8) and last (November 18) day of measurements used for this are also indicated.

3.2 Case study: Particle growth spanning a change in air mass

Figure 8 presents a set of time series for measurements made on October 10 and the morning of October 11. During this time neither chamber was perturbed, with ambient air pulled through the gas exchange channel in both and ammonium sulfate particles injected into both. The measurements during this period are interesting because they span the passage of a cold front at about 17:00 CDT, which is reflected in the abrupt changes in wind direction and speed, temperature, RH, and O_3. The size distribution and composition of the ambient aerosol also changed with the shift in air mass, with the appearance of what seems to be recently formed particles and an increase in the OA mass fraction measured by the ACSM.

The mode diameters determined from the lognormal fits of the size distributions measured in the two chambers are shown in Figure 8b and the growth rates calculated from them in Figure 8c. Immediately before the frontal passage, the particle growth rates in the two chambers were similar and generally less than about 0.3 nm hr^{-1}. After the front, particle growth rates increased significantly to between 1 and 2 nm hr^{-1}. The source of the increased growth is unknown, though the increased fractional contribution of NO_3 to the submicron aerosol may reflect condensation of NH_4NO_3 accompanying the decreased temperature. The ability to directly observe the influence of changing meteorological and chemical conditions on particle growth when doing so with measurements of the ambient aerosol is not possible is among the attributes of the CAGE system.

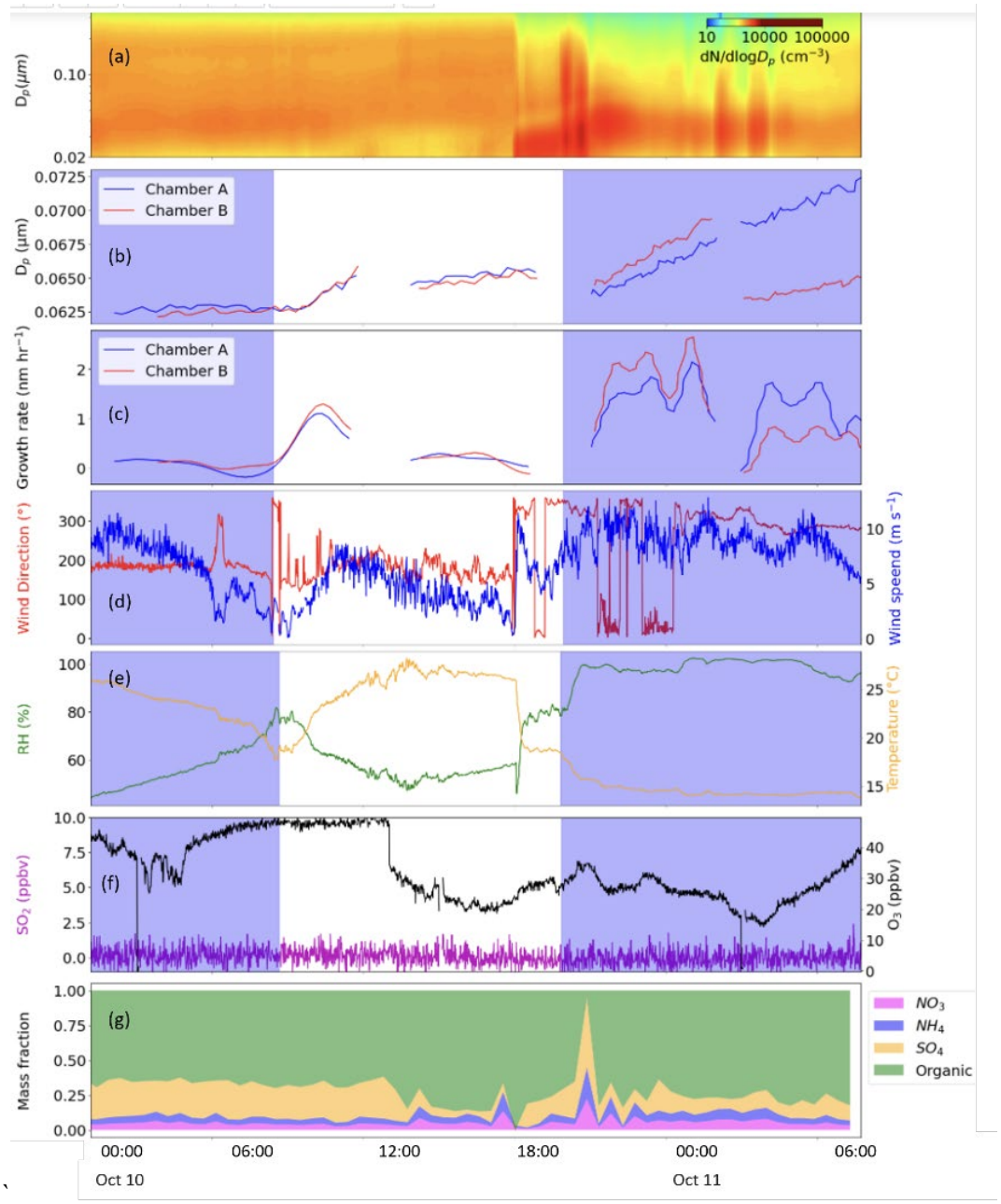

Figure 8. Differences in particle growth in distinct air masses. (a) Ambient aerosol size distribution time series, (b) time series of the lognormal fit diameters of injected modes in the two chambers, (c) calculated particle growth rates, (d) wind direction and wind speed, (e) ambient RH and temperature, (f) ambient SO_2 and O_3 mixing ratios, (g) non-refractory submicron aerosol mass fractions measured with the ACSM.

3.3 Effect of addition of precursor gases on particle growth rate

3.3.1 Effect of α-pinene on particle growth rate

Oxidation of α-pinene results in the formation of secondary organic aerosol (SOA) through equilibrium partitioning and acid-base reactions (Tröstl et al., 2016). Though the amount and properties of SOA from α-pinene oxidation have been studied extensively, those studies are typically done under tightly controlled conditions, with the gas composition and UV and visible spectra quite different from those in the environment. Contrasting the growth in reference (ambient air only) and perturbed (ambient air + α-pinene) CAGE chambers provides a measure of the sensitivity to the addition for the measurement location. The α-pinene was continuously injected from a compressed gas cylinder at a rate controlled with a mass flow controller to increase the mixing ratio in the air flushed through the gas exchange channel by 5 ppb.

Time series of the measured size distributions and resulting mode diameters and growth rates during the 2.5-day perturbation experiment are shown in Figure 9. Averaged over the experiment, the growth rate in the perturbed chamber was 4.4 nm hr^{-1}, which was significantly higher than the 0.8 nm hr^{-1} observed in the reference chamber. Variability in concentrations of oxidants and of other precursor gases and in environmental conditions resulted in a large range in the amplitude of the enhancement. Additionally, the added α-pinene triggered NPF events in the early evening of November 1 and early morning of November 2.

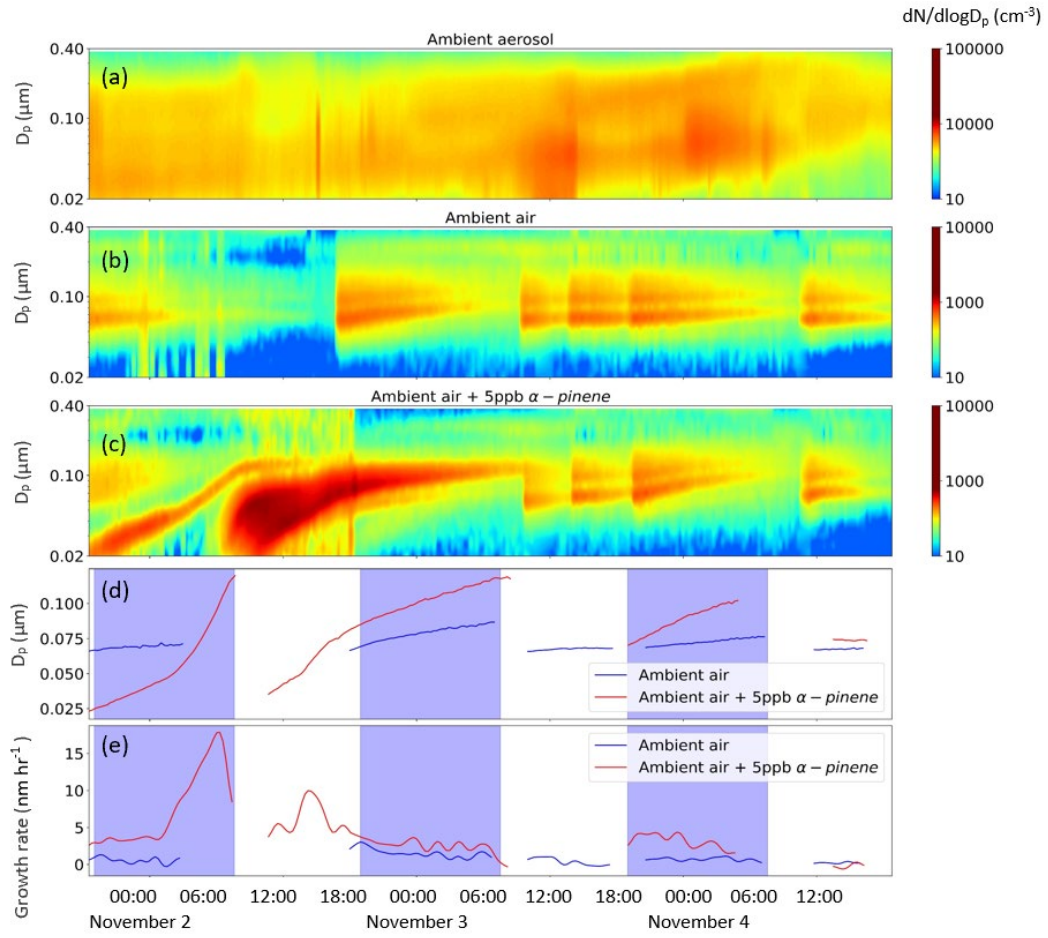

Figure 9. Time series of measurements and calculated parameters over 2.5 days during which 5 ppb of α-pinene was added to the ambient air pulled through one of the two chambers. (a) Ambient aerosol size distribution time series, (b) size distribution time series for the reference chamber, (c) size distribution time series for the perturbed chamber, (d) time series of the lognormal fit diameters of tracked modes in the two chambers, (e) particle growth rates calculated from the time series of lognormal fit diameters.

3.3.2 Effect of SO_2 on particle growth rate

Hodshire et al. (2016) reported that particle growth from condensation of H_2SO_4 that forms from gas phase oxidation of SO_2 was significant at SGP during a study in spring 2013. During the study described here, the ambient SO_2 mixing ratio was low and often at or close to the detection limit, which is at least partly a reflection of the significant downward trend in SO_2 emissions throughout the U.S. Just as was done for the α-pinene perturbation experiment, SO_2 was continuously added at a controlled rate to increase the mixing ratio of the ambient air pulled through the gas exchange channel in one of the two chambers by 5 ppb, while only ambient air was pulled through the other. Figure 10 shows the same set of time series as for the α-pinene perturbation experiment for the 4-day SO_2 perturbation.

NPF events occurred in the perturbed chamber starting at approximately 08:00 CDT on November 5 and 6. Unlike with the addition of α-pinene, which is highly reactive with both O_3 and OH, the introduction of SO_2 led to increased growth only during the daytime. The growth rate in the reference chamber varied

little throughout the period, with an average value of approximately 0.5 nm hr^{-1}. In contrast, the average daytime growth rate in the perturbed chamber was approximately 2.5 nm hr^{-1}, with the highest values observed during the two NPF events.

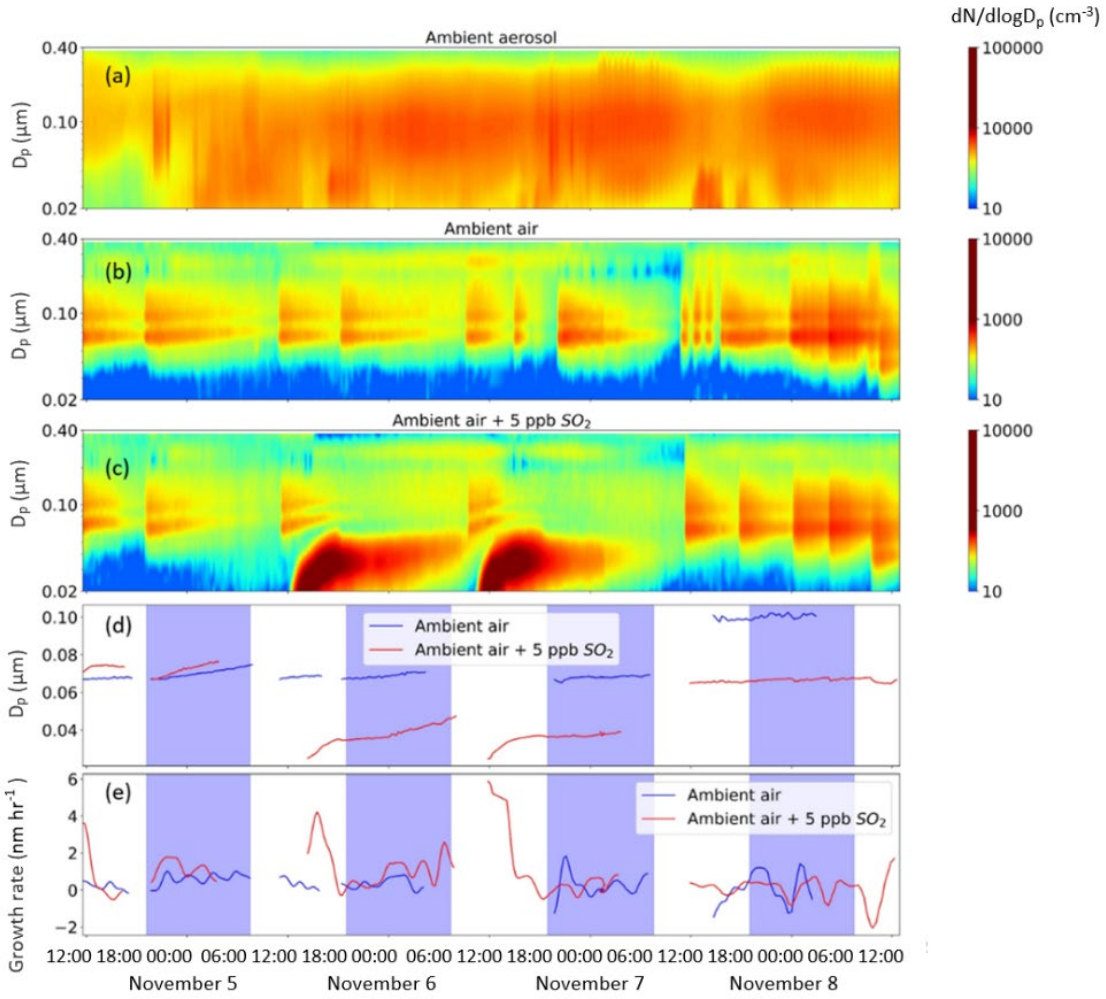

Figure 10. Time series of measurements and calculated parameters over 4 days during which 5 ppb of SO_2 was added to the ambient air pulled through one of the two chambers. (a) Ambient aerosol size distribution time series, (b) size distribution time series for the reference chamber, (c) size distribution time series for the perturbed chamber, (d) time series of the lognormal fit diameters of tracked modes in the two chambers, (e) particle growth rates calculated from the time series of lognormal fit diameters.

3.4 Effect of aerosol liquid water on particle growth rate

To examine the impact of seed particle composition and, especially, seed particle water content on secondary aerosol formation and resulting particle growth, a monodisperse mode of dry ammonium sulfate (AS) particles was injected into one chamber and one of dry potassium sulfate (KS) particles into the other. An important difference between the two seed particle types is their deliquescence RH (DRH) and efflorescence RH (ERH), with AS having a DRH of 80% and ERH of 35% (Seinfeld and Pandis, 2016) and KS having a DRH of 96% and an ERH of 60% (Freney et al., 2009). Initially crystalline particles will deliquesce if the chamber RH exceeds the DRH and will remain aqueous until the chamber

RH falls below the ERH. Particles were injected into both chambers 4 times during the 1.5-day period analyzed, as identified by the numbers above each of pair of curves in Figure 11b. At the times of the first and second injections, the chamber RH was above the DRH of AS, but below that of KS. For as long as those particle modes could be tracked, the RH did not increase above the DRH of KS or decrease below the ERH of AS. Thus, in both cases the AS particles remained aqueous and the KS particles remained crystalline. At the time of the third injection and for as long as those particle modes could be tracked, the chamber RH was below the DRH of either particle type and so both the AS and KS particles remained crystalline. At the time of the fourth injection the chamber RH was close to 100% following a period of precipitation and never fell below the ERH of either particle type for as long as the modes were tracked. Therefore, both the AS and KS particles remained aqueous. The periods during which particles of each type were aqueous are indicated by markers added to the curve segments in Figure 11b.

Following the third and fourth injections when the AS and KS particles had the same phase state, the magnitude and time-dependence of their growth were almost identical. The growth of both particle types was significantly higher when they were aqueous than when they were crystalline, though it is not possible to attribute that difference only to water content because the measurements are separated in time. The similarity in growth during those two periods suggests the seed particle composition alone (AS or KS) was relatively unimportant. In contrast, the aqueous AS particles grew substantially faster than did the crystalline KS particles following the first two injections, both during the day and at night. Specifically, for the periods of time when the AS and KS modes were tracked simultaneously, the average growth rates of the AS particles from the first and second injections were 0.41 and 0.41 nm hr^{-1}, respectively, while those of the KS particles were 0.06 and 0.16 nm hr^{-1}. Collectively, these results provide direct evidence that aerosol liquid water can have a substantial influence on secondary aerosol formation and particle growth.

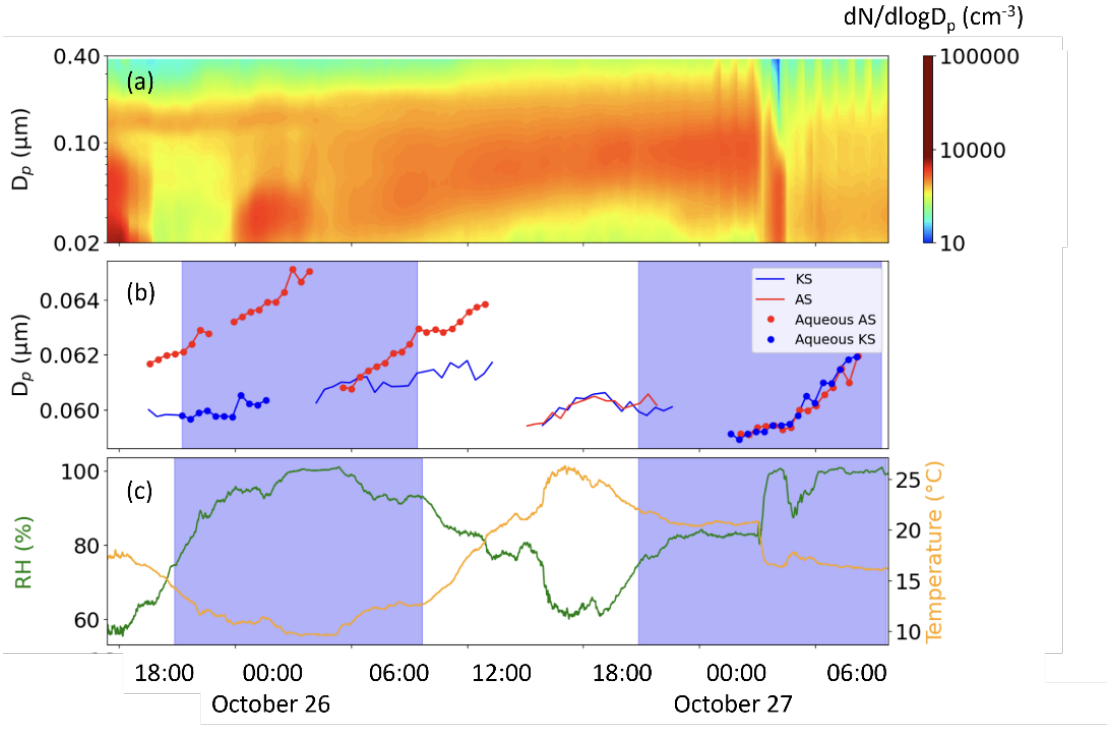

Figure 11. Time series of measurements and calculated parameters over 1.5 days during which ammonium sulfate seed particles were intermittently injected into one chamber and potassium sulfate

particles into the other. (a) Ambient aerosol size distribution time series, (b) time series of the lognormal fit diameters of particle modes in both chambers. The numbers above each pair of curves represent the injection number as described in the text. Markers on the curves indicate times when the particles were expected to be aqueous based on the injection time and chamber RH history. (c) Ambient RH and temperature.

4 Summary

Two identical Captive Aerosol Growth and Evolution (CAGE) chambers were operated at the DOE Southern Great Plains (SGP) site in the late summer and fall of 2021. CAGE chambers are designed to expose particles to an environment that mirrors that of the surroundings with or without a controlled perturbation designed to assess a sensitivity. The analysis here focuses on roughly the last two months of the overall study period during which measurements were almost continuous and when several perturbation experiments were conducted.

Though the utility of a dual-chamber system is the ability to measure the influence of a single change on top of ambient conditions, both chambers were initially operated in the same way, with ambient air pulled through the gas exchange channel in both and ammonium sulfate particles injected into both. The similar time-dependent particle growth observed in the chambers for those periods provides confidence in differences observed during the subsequent perturbation experiments. The growth rate of particles in the reference chamber into which only ammonium sulfate particles were injected and for which only ambient air was pulled through were used to describe time-of-day averages. The average growth rate was highest in the evening and in the morning after sunrise and lowest in the late afternoon.

The sensitivity of particle growth to secondary aerosol precursor gases was studied by adding them at a controlled rate to the ambient air flow pulled through one of the two chambers. Addition of 5 ppb of α-pinene resulted in an average particle growth rate of 4.4 nm hr^{-1}, compared with that of just 0.8 nm hr^{-1} in the reference chamber. The added α-pinene also triggered one NPF event in the early evening just before sunset and another in the morning just after sunrise. Similarly, addition of 5 ppb of SO_2 to one chamber led to a pair of NPF events and to increased particle growth rate, though unlike the impact of added α-pinene, growth was enhanced only during the daytime when OH concentration is highest.

The influence of aerosol liquid water on secondary aerosol formation and particle growth was investigated by injecting ammonium sulfate seed particles into one chamber and potassium sulfate particles into the other. Particles were injected into the two chambers 4 times over a 1.5-day period. The chamber RH history during and following each injection was used to determine whether each particle type was crystalline or aqueous. For the case when both particle types remained crystalline throughout the period they were tracked and for that when they remained aqueous, the magnitude and time-dependence of the growth of both were almost exactly the same. For the other two cases the ammonium sulfate particles deliquesced upon injection and remained aqueous, while the potassium sulfate particles remained crystalline. For those two cases, the aqueous particles grew by an average of 0.41 and 0.41 nm hr^{-1}, while the crystalline particles grew by only 0.06 and 0.16 nm hr^{-1}.

Boy, M., Mogensen, D., Smolander, S., Zhou, L., Nieminen, T., Paasonen, P., Plass-Dülmer, C., Sipilä, M., Petäjä, T., Mauldin, L., Berresheim, H., & Kulmala, M. (2013). Oxidation of SO_2 by stabilized Criegee intermediate (sCI) radicals as a crucial source for atmospheric sulfuric acid concentrations. *Atmospheric Chemistry and Physics*, *13*(7), 3865–3879.

Cirino, G. G., Souza, R. A. F., Adams, D. K., & Artaxo, P. (2014). The effect of atmospheric aerosol particles and clouds on net ecosystem exchange in the Amazon. *Atmospheric Chemistry and Physics*, *14*(13), 6523–6543. https://doi.org/10.5194/acp-14-6523-2014

Freney, E. J., Martin, S. T., & Buseck, P. R. (2009). Deliquescence and efflorescence of potassium salts relevant to biomass-burning aerosol particles. *Aerosol Science and Technology*, *43*(8), 799–807. https://doi.org/10.1080/02786820902946620

Goldberg, L. J. (1971). Naval Biomedical Research Laboratory, Programmed Environment, Aerosol Facility. *Applied Microbiology*. 21, 244-252.

Hao, L., Garmash, O., Ehn, M., Miettinen, P., Massoli, P., Mikkonen, S., Jokinen, T., Roldin, P., Aalto, P., Yli-Juuti, T., Joutsensaari, J., Petäjä, T., Kulmala, M., Lehtinen, K. E. J., Worsnop, D. R., & Virtanen, A. (2018). Combined effects of boundary layer dynamics and atmospheric chemistry on aerosol composition during new particle formation periods. *Atmospheric Chemistry and Physics*, *18*(23), 17705–17716. https://doi.org/10.5194/acp-18-17705-2018

Hirsikko, A., Vakkari, V., Tiitta, P., Manninen, H. E., Gagné, S., Gagné, S., Laakso, H., Kulmala, M., Mirme, A., Mirme, S., Mabaso, D., Beukes, J. P., & Laakso, L. (2012). Characterisation of sub-micron particle number concentrations and formation events in the western Bushveld Igneous Complex, South Africa. *Atmospheric Chemistry and Physics*, *12*(9), 3951–3967. https://doi.org/10.5194/acp-12-3951-2012

Hodshire, A. L., Lawler, M. J., Zhao, J., Ortega, J., Jen, C., Yli-juuti, T., Brewer, J. F., Kodros, J. K., Barsanti, K. C., Hanson, D. R., McMurry, P. H., Smith, J. N., & Pierce, J. R. (2016). Multiple new-particle growth pathways observed at the US DOE Southern Great Plains field site. *Atmospheric Chemistry and Physics*, 9321–9348.

Huang, W., Saathoff, H., Shen, X., Ramisetty, R., Leisner, T., & Mohr, C. (2019). Chemical Characterization of Highly Functionalized Organonitrates Contributing to Night-Time Organic Aerosol Mass Loadings and Particle Growth. *Environmental Science and Technology*, *53*(3), 1165–1174. https://doi.org/10.1021/acs.est.8b05826

Jaenicke, R. (1980). ATMOSPHERIC AEROSOLS AND GLOBAL CLIMATE. In *J Aerosol Sci* (Vol. 11). Pergamon Press Ltd.

Kerminen, V. (2018). Atmospheric new particle formation and growth: review of field observations Atmospheric new particle formation and growth: review of field observations. Environmental Research Letters. doi.org/10.1088/1748-9326/aadf3c.

Kulmala, M., Petäjä, T., Ehn, M., Thornton, J., Sipilä, M., Worsnop, D. R., & Kerminen, V. M. (2014). Chemistry of atmospheric nucleation: On the recent advances on precursor characterization and atmospheric cluster composition in connection with atmospheric new particle formation. *Annual Review of Physical Chemistry*, *65*, 21–37. https://doi.org/10.1146/annurev-physchem-040412-110014

Liu, J., Alexander, L., Fast, J. D., Lindenmaier, R., & Shilling, J. E. (2021). Aerosol characteristics at the Southern Great Plains site during the HI-SCALE campaign. 5101–5116.

McNeill, V. F. (2017). *Atmospheric Aerosols: Clouds, Chemistry, and Climate*. https://doi.org/10.1146/annurev-chembioeng

Misson, L., Lunden, M., McKay, M., & Goldstein, A. H. (2005). Atmospheric aerosol light scattering and surface wetness influence the diurnal pattern of net ecosystem exchange in a semi-arid ponderosa pine plantation. *Agricultural and Forest Meteorology*, *129*(1–2), 69–83. https://doi.org/10.1016/j.agrformet.2004.11.008

Parworth, C., Fast, J., Mei, F., Shippert, T., Sivaraman, C., Tilp, A., Watson, T., & Zhang, Q. (2015). Long-term measurements of submicrometer aerosol chemistry at the Southern Great Plains (SGP) using an Aerosol Chemical Speciation Monitor (ACSM). *Atmospheric Environment*, *106*, 43–55. https://doi.org/10.1016/j.atmosenv.2015.01.060

Pöschl, U. (2005). Atmospheric aerosols: Composition, transformation, climate and health effects. In *Angewandte Chemie - International Edition* (Vol. 44, Issue 46, pp. 7520–7540). https://doi.org/10.1002/anie.200501122

Sirmollo, C. L., Collins, D. R., McCormick, J. M., Milan, C. F., Erickson, M. H., Flynn, J. H., Sheesley, R. J., Usenko, S., Wallace, H. W., Bui, A. A. T., Griffin, R. J., Tezak, M., Kinahan, S. M., and Santarpia, J. L.: Captive Aerosol Growth and Evolution (CAGE) chamber system to investigate particle growth due to secondary aerosol formation, Atmos. Meas. Tech., 14, 3351–3370, https://doi.org/10.5194/amt-14-3351-2021, 2021.

Stolzenburg, M., Kreisberg, N., & Hering, S. (1998). Atmospheric Size Distributions Measured by Differential Mobility Optical Particle Size Spectrometry. *Aerosol Science and Technology*, *29*(5), 402–418. https://doi.org/10.1080/02786829808965579

Tröstl, J., Chuang, W. K., Gordon, H., Heinritzi, M., Yan, C., Molteni, U., Ahlm, L., Frege, C., Bianchi, F., Wagner, R., Simon, M., Lehtipalo, K., Williamson, C., Craven, J. S., Duplissy, J., Adamov, A., Almeida, J., Bernhammer, A. K., Breitenlechner, M., … Baltensperger, U. (2016). The role of low-volatility organic compounds in initial particle growth in the atmosphere. *Nature*, *533*(7604), 527–531. https://doi.org/10.1038/nature18271

Viana, M., Pey, J., Querol, X., Alastuey, A., de Leeuw, F., & Lükewille, A. (2014). Natural sources of atmospheric aerosols influencing air quality across Europe. *Science of the Total Environment*, *472*, 825–833. https://doi.org/10.1016/j.scitotenv.2013.11.140

Wimmer, D., Buenrostro Mazon, S., Manninen, H. E., Kangasluoma, J., Franchin, A., Nieminen, T., Backmann, J., Wang, J., Kuang, C., Krejci, R., Brito, J., Goncalves Morais, F., Martin, S. T., Artaxo, P., Kulmala, M., Kerminen, V.-M., & Petäjä, T. (2017). Direct observation of molecular clusters and nucleation mode particles in the Amazon. *Atmospheric Chemistry and Physics Discussions*, *August*, 1–37.